

1 Summary

We re-investigate the electromagnetic (EM) core-mantle coupling, for which the geomagnetic field, B , at the core-mantle boundary (CMB) must be known. One motivation is that we can infer the poloidal magnetic field at the CMB from its surface representations by the method of non-harmonic downward continuation (NHDC) through an electrically conducting mantle (Ballani *et al.*, 2002; see also poster session JAS004). The computation of the EM coupling torque, L , is then based on a rigorous numerical inversion of the mantle induction equation.

B can be split into poloidal and toroidal parts, B^P and B^T , respectively. The associated parts of the EM coupling torque are then commonly denoted as poloidal and toroidal torque, L^P and L^T , respectively. This splitting defines two different problems of the field computation at the CMB. Whereas B^P can be completely inferred from the observed and downward continued geomagnetic field, B^T can only be computed at the CMB using some model constraints shown in section 3. The second motivation for the re-investigation is that we will numerically solve the induction equation for B^T in the conducting part of the mantle.

For the computation of the CMB field, we use magnetic field expansion into spherical harmonics (SH) of Wardinski & Holme (2006). For the conductivity, σ_m , we assume a small shell at the CMB of constant conductivity, and an rapid exponential decrease at its upper edge. To compute the boundary values of B^T at the CMB, we used the velocity field u_{CMB} according to Wardinski (2005).

The application of the NHDC has required to re-write the torque expressions and the numerics. We show:

- analytical expressions of L^P and L^T in dependence on B^P and B^T and their SH coefficients at the CMB
- the boundary value problem for B^T and its solution
- an example for u_{CMB} consistent with NHDC
- results of a numerical test for L for the interval 1986 – 1996

3 Toroidal magnetic field

For the computation of the torque, the fields S and T are needed at the CMB:

- $S(R_{CMB}) \rightarrow$ by NHDC (inverts $\Delta S = \mu_0 \sigma_M \dot{S}$)
- $T(R_{CMB}) \rightarrow$ by velocity field u_{CMB} and

the induction equation for T

$$\Delta T - \frac{1}{\sigma_M} \frac{d\sigma_M}{dr} \frac{\partial(rT)}{\partial r} = \mu_0 \sigma_M \frac{\partial T}{\partial t} \quad r \in [R_{CMB}^+, R_\sigma]$$

with the boundary conditions (BC)

$$\begin{aligned} T &= 0 & \text{at } r &= R_\sigma \\ T &= T_{CMB} & \text{at } r &= R_{CMB}^+ \end{aligned}$$

The continuity of $r \times E$ at the CMB gives an additional BC

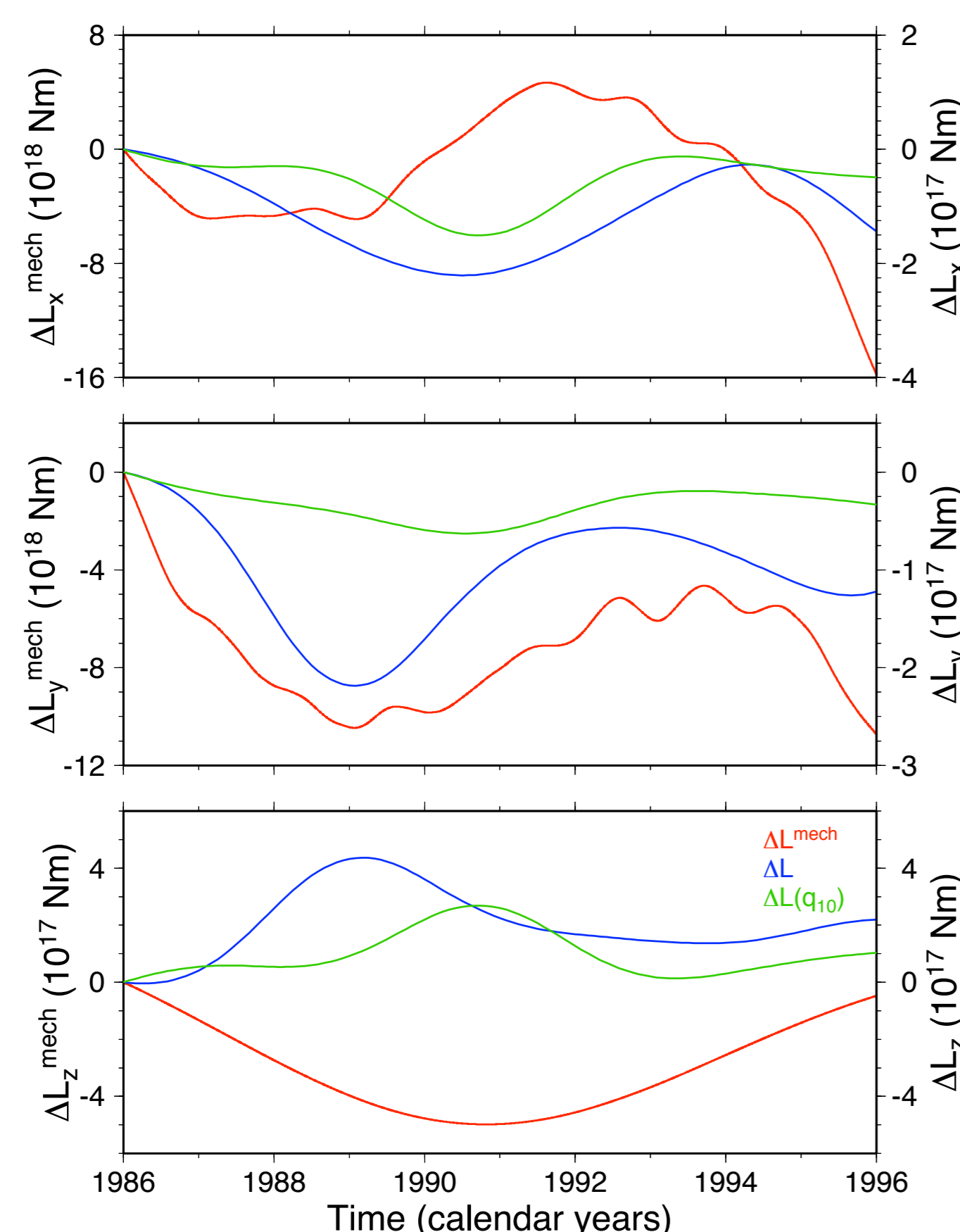
$$\frac{\sigma_M}{\sigma_C} \left[\frac{\partial}{\partial r} (rT) \right]_{CMB}^- - \left[\frac{\partial}{\partial r} (rT) \right]_{CMB}^+ = \mu_0 \sigma_M W(u, B)$$

T_{CMB} is obtained from the solution of the induction equation with the additional BC and $T(R_\sigma) = 0$. The SH coefficients of W are given by

$$\begin{aligned} W_{jm} &= \frac{-1}{j(j+1)} \int_{\Omega} r [\nabla \times (r \times (u \times B))] Y_{jm}^*(\Omega) d\Omega \\ W_{jm} &= \frac{-1}{j(j+1)} \sum_{klst} k(k+1) S_{kl}^{jm} [L_{klst}^{jm} p_{st}(t) - K_{klst}^{jm} q_{st}(t)] \end{aligned}$$

where p_{st}, q_{st} are the SH coefficients of u_{CMB} and $K_{klst}^{jm}, L_{klst}^{jm}$ denote the coupling integrals, expressible by Clebsch-Gordan coefficients (see eqs. (5) and (6) below).

6 Resulting EM torques



← **Figure 2:** Comparison of ΔL^{mech} and ΔL for the test interval 1986 – 1996. In addition ΔL is shown, which is computed with a simple westward drift of the fluid flow at the CMB represented by a single time dependent velocity coefficient $q_{10}(t)$. All components of ΔL are computed from the related components of L by de-trending the time series with respect to their values at the begin of the year 1986.

7 Discussion and conclusions

• Comparison of ΔL for different fluid flow

Considering a simple westward drift instead of a complex fluid flow at the CMB leads to a smaller EM coupling torque (only $\sim 50\%$). Moreover, the time behavior is quite different in all components, with respect to amplitude and phase. This significant differences illustrate the dependence of the resulting EM coupling torque on the computed fluid flow velocity u_{CMB} , which is dependent on different assumptions, because of the non-uniqueness of the fluid flow inversion.

• Comparison of ΔL and ΔL^{mech}

Only the axial components of ΔL_z and ΔL_z^{mech} are in the same order of magnitude, but differ significantly in the time behavior by a phase shift of their extrema. In contrast, the non-axial components of the EM coupling torque ΔL are at least smaller by a factor of ~ 40 than the computed mechanical torque. For ΔL_y component does not exist a significant phase shift to the mechanical torque, whereas for the ΔL_x component this is clearly detectable.

2 Electromagnetic torques

Lorentz torque on the mantle

$$L = \frac{1}{\mu_0} \int_V r \times (\text{rot } B \times B) dV$$

Poloidal-toroidal decomposition of the magnetic field by the scalar function S and T

$$B = B^P + B^T \quad B = \text{rot rot}(rS) + \text{rot}(rT)$$

and the related SH representation with $Y_{jm}(\Omega)$ (Varshalovich *et al.*, 1989)

$$S = \sum_{j=1}^{j_{\max}} \sum_{m=-j}^j S_{jm} Y_{jm}(\Omega) \quad T = \sum_{j=1}^{j_{\max}} \sum_{m=-j}^j T_{jm} Y_{jm}(\Omega)$$

2.1 Poloidal torques

Axial poloidal EM coupling torque

$$L_z^P = \frac{R_{CMB}}{\mu_0} \int_{\Omega} \Delta_{\Omega} S \frac{\partial^2}{\partial \varphi \partial r} (rS) d\Omega$$

where the Laplace Operator on a sphere is given by

$$\Delta_{\Omega} = \left[\frac{1}{\sin \vartheta} \frac{\partial}{\partial \vartheta} \left(\sin \vartheta \frac{\partial}{\partial \vartheta} \right) + \frac{1}{\sin^2 \vartheta} \frac{\partial^2}{\partial \varphi^2} \right]$$

where the SH representation is given by eq. (1)

Non-axial poloidal EM coupling torques

$$\begin{aligned} L_x^P &= -\frac{R_{CMB}}{\mu_0} \int_{\Omega} \Delta_{\Omega} S \left(\cot \vartheta \cos \varphi \frac{\partial^2}{\partial \varphi \partial r} (rS) + \sin \varphi \frac{\partial^2}{\partial \vartheta \partial r} (rS) \right) d\Omega \\ L_y^P &= -\frac{R_{CMB}}{\mu_0} \int_{\Omega} \Delta_{\Omega} S \left(\cot \vartheta \sin \varphi \frac{\partial^2}{\partial \varphi \partial r} (rS) - \cos \varphi \frac{\partial^2}{\partial \vartheta \partial r} (rS) \right) d\Omega \end{aligned}$$

used as complex combination

$$L^P = L_x^P + i L_y^P$$

where the SH representation is given by eq. (2)

2.2 Toroidal torques

Axial toroidal EM coupling torque

$$L_z^T = -\frac{R_{CMB}^2}{\mu_0} \int_{\Omega} \Delta_{\Omega} S \sin \vartheta \frac{\partial}{\partial \vartheta} T d\Omega$$

where the SH representation is given by eq. (3)

Non-axial toroidal EM coupling torques

$$\begin{aligned} L_x^T &= -\frac{R_{CMB}^2}{\mu_0} \int_{\Omega} \Delta_{\Omega} S \left(\frac{\sin \varphi}{\sin \vartheta} \frac{\partial}{\partial \varphi} T - \cos \vartheta \cos \varphi \frac{\partial}{\partial \vartheta} T \right) d\Omega \\ L_y^T &= \frac{R_{CMB}^2}{\mu_0} \int_{\Omega} \Delta_{\Omega} S \left(\frac{\cos \varphi}{\sin \vartheta} \frac{\partial}{\partial \varphi} T + \cos \vartheta \sin \varphi \frac{\partial}{\partial \vartheta} T \right) d\Omega \end{aligned}$$

used as complex combination

$$L^T = L_x^T + i L_y^T$$

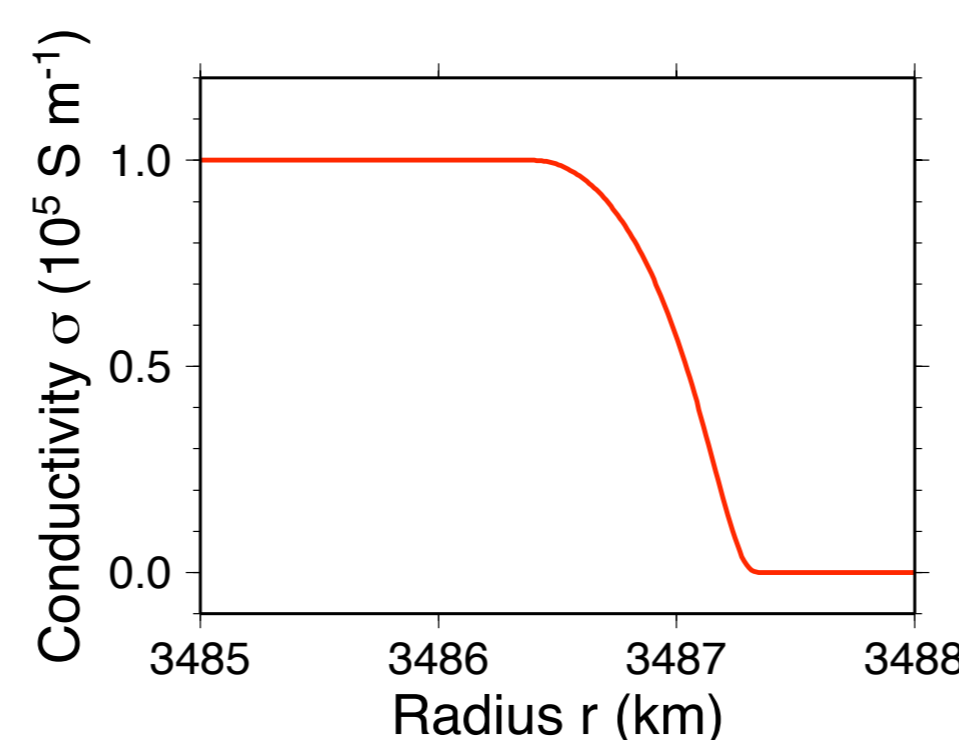
where the SH representation is given by eq. (4)

For the first practical calculations we have solved the induction equation for the quasi-stationary case and neglected the first term in the additional BC, i.e. considered the generation of the toroidal field at the CMB by advection only.

4 Conductivity model and data

• Conductivity model

$$\sigma_M(r) = \begin{cases} 10^5 \text{ S m}^{-1} & \text{for } R_{CMB} < r < R_s \\ c \exp\left(\frac{-1}{1 - ((R_s - r)/s)^2}\right) \text{ S m}^{-1} & \text{for } R_s \leq r \leq R_\sigma \\ 0 \text{ S m}^{-1} & \text{for } r > R_\sigma \end{cases}$$



$$\begin{aligned} R_{CMB} &= 3485.0 \text{ km} \\ R_s &= 3486.4 \text{ km} \\ R_\sigma &= 3487.4 \text{ km} \\ c &= 2.71828 \cdot 10^5 \\ s &= 1.0 \text{ km} \end{aligned}$$

• Magnetic data

Gauss coefficients $g_{jm}(t), h_{jm}(t)$ by Wardinski & Holme (2005) for $j_{\max} = 8$, which were re-normed and combined to complex $S_{jm}(t)$.

• EOP and AAM data

Time series of earth orientation parameter (EOP: C04) and the atmospheric angular momentum (AAM: NCEP-NCAR) are obtained from IERS (see also: <http://hpiers.obspm.fr/eop-pc/analysis/excitative.htm>).

• Mechanical torques

Computed by numerical solving of the linearized Liouville equation for the torque, using the EOP and AAM data.

5 Core flow

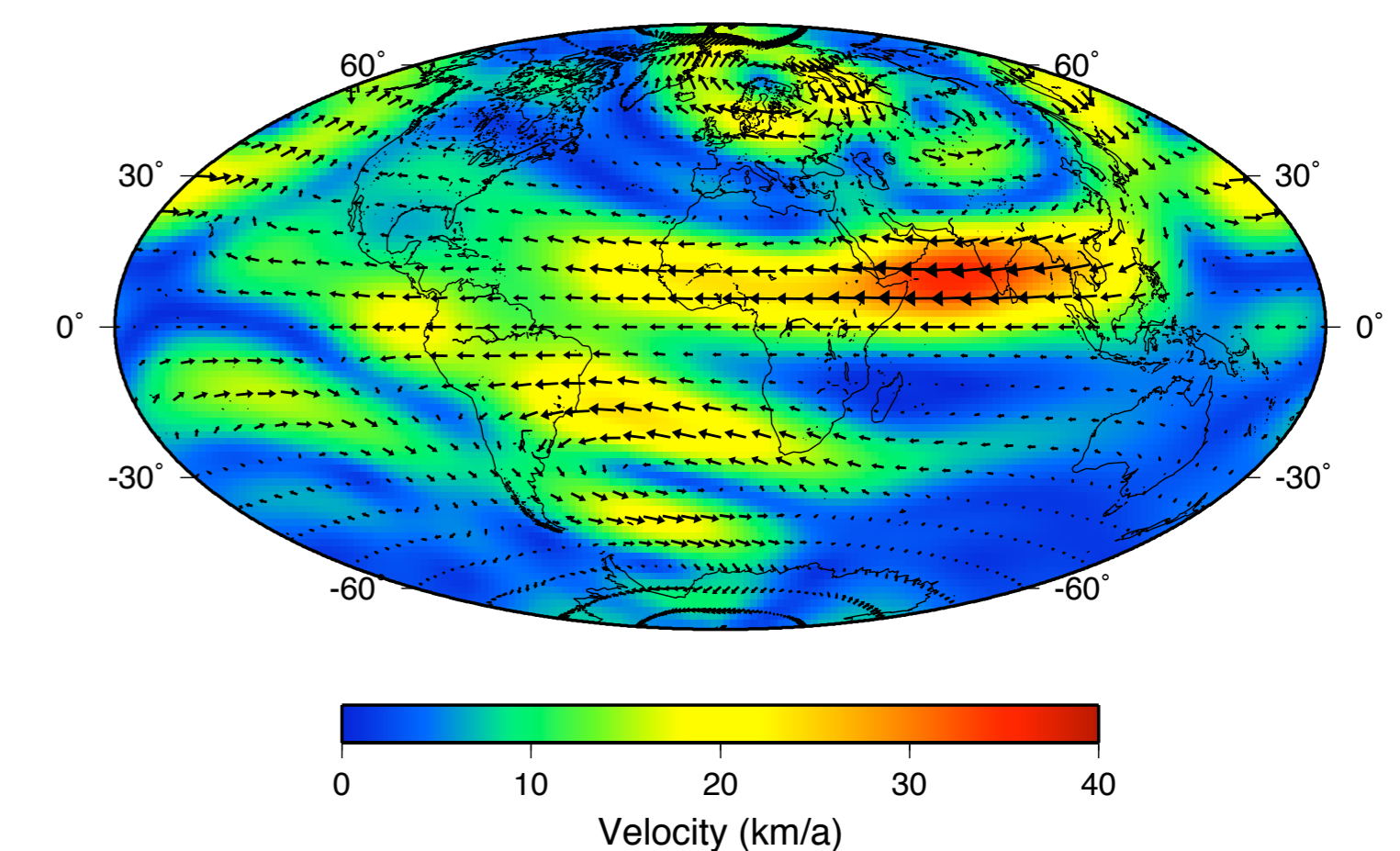


Figure 1: Velocity u_{CMB} at the CMB calculated by I. Wardinski from $S(R_{CMB})$ by NHDC for the year 1990. For the computation the constraint of tangential geostrophy is used, according to Wardinski (2005).

• Additional core-mantle coupling mechanism

The significant differences between the mechanical and EM coupling torques give a hint for missing additional core-mantle coupling mechanism, as gravitational and topographic coupling. Besides further theoretical developments for a non-stationary induction equation for the toroidal magnetic field, we want to extend in a consistent way the description of the core-mantle coupling for this additional mechanism. The non-uniqueness of the fluid flow should also be considered in this further investigations.

References

- Ballani, L., Greiner-Mai, H. and Stromeyer, D., 2002. Determining the magnetic field in the core-mantle-boundary zone by non-harmonic downward continuation. *Geoph. J. Int.*, **149**, 374-389.
- Ballani, L., Stromeyer, D., Greiner-Mai, H. and Hagedoorn, J., 2007. The non-harmonic downward continuation method in deep earth magnetic field studies. Poster Session JAS004. IUGG 2007.
- Varshalovich, D., Moskalev, A. and Khersonskii, V., 1989. *Quantum Theory of Angular Momentum*. World Scientific, Singapore.
- Wardinski, I., 2005. Core surface flow models from decadal and subdecadal variation of the main geomagnetic field. *Sci. Tech. Rep.*, STR 05/07, GFZ Potsdam.
- Wardinski, I. and Holme, R., 2006. A time-dependent model of the earth's magnetic field and its secular variation for the period 1980 to 2000. *J. Geophys. Res.*, **111**, doi:10.1029/2006JB004401.

E-mail jan@gfz-potsdam.de

$$L_z^P = \frac{R_{CMB}}{\mu_0} \sum_{j=1}^{j_{\max}} \sum_{m=-j}^j m j(j+1) i \left[S_{jm} \frac{\partial}{\partial r} S_{jm}^* - S_{jm}^* \frac{\partial}{\partial r} S_{jm} \right] \quad (1)$$

$$L^P = \frac{i R_{CMB}}{\mu_0} \sum_{j=1}^{j_{\max}} j(j+1) \left\{ \sqrt{j(j+1)} S_{j1}^* \left(S_{j1} + R_{CMB} \frac{\partial}{\partial r} S_{j1} \right) + \sum_{m=2}^j \left[\sqrt{j(j+1) - m(m+1)} S_{jm}^* \left(S_{jm} + R_{CMB} \frac{\partial}{\partial r} S_{jm} \right) - \sqrt{j(j+1) - m(m-1)} S_{jm}^* \left(S_{j,m-1} + R_{CMB} \frac{\partial}{\partial r} S_{j,m-1} \right) \right] \right\} \quad (2)$$

$$L_z^T = -\frac{R_{CMB}^2}{\mu_0} \sum_{j=1}^{j_{\max}} j(j+1) \left\{ (j-1) \sqrt{\frac{j-1}{(2j+1)(2j-1)}} S_{j0}^* T_{j0} + \sum_{m=1}^j \left[\sqrt{\frac{j+1}{(2j+3)(2j+1)}} S_{jm}^* T_{j,m+1} + \sqrt{\frac{j+1}{(2j+1)(2j-1)}} S_{jm}^* T_{j,m-1} \right] - (j+2) \sqrt{\frac{j+1}{(2j+3)(2j+1)}} \left(S_{j0}^* T_{j0} + S_{j2}^* T_{j2} \right) \right\} \quad (3)$$

$$L^T = -\frac{R_{CMB}^2}{\mu_0} \sum_{j=1}^{j_{\max}} j(j+1) \left\{ S_{j0}^* \left[\frac{j(j-1)^2}{(2j-1)} T_{j0} + \frac{j+1}{(2j+3)} T_{j0} \right] + \sum_{m=1}^j \left[S_{jm}^* \left(\frac{j-m}{(2j-1)} T_{j,m+1} + \frac{j+m+2}{(2j+3)} T_{j,m+1} \right) - S_{jm}^* \left(\frac{j+m}{(2j-1)} T_{j,m-1} + \frac{j-m+2}{(2j+3)} T_{j,m-1} \right) \right] \right\} \quad (4)$$

$$K_{klst}^{jm} = \frac{1}{2} [k(k+1) - s(s+1) - j(j+1)] \sqrt{\frac{(2k+1)(2s+1)}{4\pi(2j+1)}} C_{klst}^{jm} \quad (5)$$

$$L_{klst}^{jm} = \frac{1}{2} \sqrt{(k+s+j+2)(k-s-j)(k-s+j+1)(-k+s+j+1)} \sqrt{\frac{(2k+1)(2s+1)}{4\pi(2j+3)}} C_{klst}^{jm} \quad (6)$$

where C_{klst}^{jm} denotes the Clebsch-Gordan coefficients (Varshalovich, 1989)